

WWLLN Energetic Lightning Events are Different from Optical Superbolts

Michael Jay Peterson¹

¹ISR-2, Los Alamos National Laboratory

April 16, 2023

Abstract

The most powerful optical emissions from lightning have been described as “superbolts” since the 1970s. In 2019, Holzworth et al. (2019) applied the superbolt label to the most energetic Radio Frequency (RF) emissions measured by the World Wide Lightning Location Network (WWLLN). In this study, we compare the WWLLN energies to optical measurements by the photodiode detector (PDD) on the Fast On-orbit Recording of Transient Events (FORTE) satellite and the Geostationary Lightning Mappers (GLMs) on NOAA’s Geostationary Operational Environmental Satellites (GOES) to assess whether WWLLN high energy events coincide with optical superbolts. We find no overlap between traditional superbolts and WWLLN high energy events. Optical superbolts are not energetic to WWLLN, while WWLLN superbolts are not optically bright. Additionally, the top WWLLN sources occur in a different meteorological context than superbolts. Despite some similarities in their overall global patterns of occurrence, WWLLN high energy events correspond to a different phenomenon.

WWLLN Energetic Lightning Events are Different from Optical Superbolts

Michael Peterson¹

¹ ISR-2, Los Alamos National Laboratory, Los Alamos, New Mexico

Corresponding author: Michael Peterson (mpeterson@lanl.gov)

Key Points:

- Optical and WWLLN VLF energies are compared in superbolt and high WWLLN energy cases
- Optical superbolts are associated with large megaflashes typically found in stratiform clouds and do not reach the WWLLN 1 MJ threshold
- WWLLN high energy events do not produce strong optical flashes, and arise in convective thunderstorm cores with low flash rates

18 **Abstract**

19 The most powerful optical emissions from lightning have been described as “superbolts”
20 since the 1970s. In 2019, Holzworth et al. (2019) applied the superbolt label to the most
21 energetic Radio Frequency (RF) emissions measured by the World Wide Lightning Location
22 Network (WWLLN). In this study, we compare the WWLLN energies to optical measurements
23 by the photodiode detector (PDD) on the Fast On-orbit Recording of Transient Events (FORTE)
24 satellite and the Geostationary Lightning Mappers (GLMs) on NOAA’s Geostationary
25 Operational Environmental Satellites (GOES) to assess whether WWLLN high energy events
26 coincide with optical superbolts. We find no overlap between traditional superbolts and
27 WWLLN high energy events. Optical superbolts are not energetic to WWLLN, while WWLLN
28 superbolts are not optically bright. Additionally, the top WWLLN sources occur in a different
29 meteorological context than superbolts. Despite some similarities in their overall global patterns
30 of occurrence, WWLLN high energy events correspond to a different phenomenon.

31

32 **Plain Language Summary**

33 Where do the most powerful lightning signals on Earth come from? The answer depends
34 on the wavelength of radiation being measured. We typically use the flashes of optical light
35 produced by lightning to make that assessment. These top cases are known as “superbolts” and
36 typically arise from long-horizontal discharges that we call “megaflashes,” which are very
37 effective light sources. A recent study by Holzworth et al. (2019) used radio waves in the Very
38 Low Frequency (VLF) band recorded by the World Wide Lightning Location Network
39 (WWLLN) to assess lightning intensity. While they call their most energetic events superbolts,
40 our comparisons with optical sensors show that they are a distinct phenomenon. WWLLN high
41 energy events come from small flashes in the thunderstorm core rather than megaflashes outside
42 of convection. We hypothesize factors that give rise to WWLLN high energy events, which need
43 to be investigated in future work.

44

45 **1 Introduction**

46 In the heart of the Cold War, Turman (1977) published lightning observations from the
47 United States’ Vela satellite constellation in the scientific literature. The lightning reported by
48 Turman (1977) was not the standard collection of flashes that would later be observed by optical
49 satellite-based sensors to construct the space-based lightning climatologies (Christian et al.,
50 2003, Albrecht et al., 2016, Peterson et al., 2021) used in physical research today. Instead,
51 Turman (1977) focused on the most powerful optical emissions generated by lightning – which
52 he termed “superbolts.”

53 Turman (1977) found that superbolts had peak optical powers two orders of magnitude
54 greater than ordinary lightning – radiating an estimated $10^{11} - 10^{12}$ W at the source with total
55 energies integrated over the pulse exceeding 10^8 J. Turman (1977) also noted that superbolts
56 have a distinct pattern of occurrence that differs from normal lightning. 9-in-10 lightning flashes
57 are produced by convective thunderstorms (Peterson and Liu, 2011) that arise as a consequence
58 of atmospheric instability and local lifting mechanisms in regions with adequate moisture. For
59 this reason, there are global lightning “hotspots” (Albrecht et al., 2016) in locations on the Earth
60 where favorable conditions are frequently met. These so-called lightning “chimneys” are found

61 in the tropics, and include Lake Maracaibo in South America, the Congo Basin in Africa, and the
62 Maritime Continent in Asia (Whipple and Scrase, 1936; references in Williams, 2005).

63 In contrast to ordinary lightning, Turman's superbolts occur in environments that are
64 unfavorable for lightning production: mid-latitude cold-season storms with a notable hotspot in
65 the seas surrounding near Japan. This distinction implies that superbolts are not merely the tip of
66 the optical power spectrum from normal lightning, but rather a rare class of discharge enabled by
67 the unique environment in which they form. Turman (1977) and subsequent comments
68 speculated on the origins of these events, but investigations were limited by the available
69 measurements of the era.

70 Advances in lightning detection since Turman's 1977 study are allowing us to clarify the
71 origins of this extreme yet incredibly rare lightning. In 1997, the Fast On-orbit Recording of
72 Transient Events (FORTE: Light, 2020) satellite was launched that included a photodiode
73 detector (PDD: Kirkland et al., 2001) capable of identifying the superbolts described by Turman
74 (1977). The Low Earth Orbit (LEO) of FORTE limited its observations to minute-scale
75 thunderstorm snapshots, making it unlikely for a superbolt to occur within the PDD Field of
76 View (FOV) while the satellite was overhead. Over a period of 12 years in orbit, FORTE found
77 itself in the right place at the right time to observe tens of thousands of 10^{11} W events, and
78 dozens of terawatt-class superbolts. Ground-based lightning detection networks were also
79 improving and becoming more ubiquitous during the FORTE mission. We used observations by
80 the National Lightning Detection Network (NLDN: Cummins and Murphy, 2009) to confirm that
81 the more powerful superbolts (> 350 MW) over the United States were commonly produced by
82 high peak current positive Cloud-to-Ground (CG) lightning strokes (Peterson and Kirkland,
83 2020).

84 Our subsequent analyses with NOAA's Geostationary Lightning Mappers (GLMs:
85 Rudlosky et al., 2019) – optical lightning detectors on the Geostationary Operational
86 Environmental Satellites (GOES) – also linked the most energetic superbolts to long-horizontal
87 lightning “megaflashes” that propagate through expansive electrified clouds outside of the
88 convective thunderstorm core (Peterson and Lay, 2020). We hypothesize that superbolts arise as
89 a consequence of these extensive networks of lightning channels that are efficient at mobilizing
90 vast quantities of charge from across a large reservoir while serving as extended optical sources
91 (rather than the typical point sources) whose individual channel segments all contribute to the
92 total optical output.

93 Towards the end of the FORTE PDD record (April 2009 and onward), the World Wide
94 Lightning Location Network (WWLLN) began saving the required station data to compute the
95 far-radiated Very Low Frequency (VLF)-band Radio Frequency (RF) energies from lightning
96 strokes. This radiation propagates in the Earth-ionosphere waveguide with low attenuation over
97 distances up to thousands of kilometers from the source to WWLLN receivers distributed across
98 the globe. Attenuation is corrected using the U.S. Navy's Long Wavelength Propagation
99 Capability code (see Thomson, 2010) to estimate the energy of the source in the 5-18 kHz band.

100 Holzworth et al. (2019) used these WWLLN energies to identify the top emitters in the
101 VLF band and labeled these lightning events “superbolts.” Their justification for making this
102 assessment based on VLF energy, alone, was that some of the top WWLLN strokes showed a
103 similar pattern of occurrence to the Vela and FORTE superbolt distributions – including a

104 wintertime mid-latitude maximum. They did not correlate WWLLN VLF energies with optical
105 outputs or offer a hypothesis for the cause of extreme WWLLN events.

106 We must be careful with any assumption that extreme RF output implies exceptional
107 optical output because the two phenomenologies are sensitive to different aspects of the lightning
108 discharge. Optical emissions that escape to space are created by the extreme heating of the
109 lightning channels in the clouds, where the atmospheric constituent gasses go through
110 dissociation, excitation, and recombination to produce particularly strong signals in certain
111 spectral bands (the 777.4 nm band used by GLM is an Oxygen line triplet). These signals are
112 then attenuated by absorption and scattering in the clouds, which reduces the contributions from
113 low altitudes (Thomas et al., 2000).

114 RF emissions, meanwhile, are generated by the movement of charge through the
115 lightning channels. WWLLN's VLF receivers are particularly sensitive to large transient currents
116 (Cummins and Murphy, 2009), while factors that are important for optical emission (i.e., cloud
117 scattering, horizontal channel dimensions) are not important for WWLLN. The extensive
118 comparisons between optical and VHF-band RF emissions in the literature demonstrate why
119 conflating RF and optical outputs may not be appropriate. The most powerful natural emitters of
120 VHF radiation are Compact Intracloud Discharges (CIDs) – lightning events within
121 thunderclouds that are inferred to have short (< 1 km) channel lengths dominated by cold
122 streamers rather than hot leaders. As a result, the top VHF events at the tip of the lightning power
123 spectrum produce little, if any, optical emissions in the common spectral bands for lightning
124 detection (Light and Jacobson, 2002). While perhaps not to the extreme extent of VHF, there
125 may still be a disconnect between VLF and optical lightning outputs.

126 Assessing whether the most energetic WWLLN events correspond to optical superbolts
127 requires direct comparisons between the optical and VLF outputs from lightning events. In this
128 study, we identify WWLLN strokes jointly detected by either the FORTE PDD or GLM, and
129 compare the emissions between each phenomenology.

130

131 **2 Data and Methods**

132 **2.1 The World Wide Lightning Location Network (WWLLN)**

133 WWLLN consists of ~80 VLF sensors across the globe that detect atmospheric
134 electromagnetic impulses generated by lightning. Waveforms within a band extending from 100
135 Hz to 24 kHz are recorded at each station and used to determine the Time of Group Arrival
136 (TOGA) of the incident radiation (Dowden et al., 2002) with an accuracy of ~1 μ s. The energies
137 reported by WWLLN are derived from this station data, using a 5-18 kHz sub-band within the
138 broadband signal. The TOGAs from each station in the network are compared to identify joint
139 detections of the same lightning stroke. Whenever five or more WWLLN stations detect a stroke,
140 their locations and arrival times are used to compute the location of the stroke on the Earth.
141 Generally, WWLLN stroke locations are considered accurate to within ~10 km (Abarca et al.,
142 2010).

143 Holzworth et al. (2019) identifies high energy events as WWLLN strokes with (1)
144 reported energies > 1 MJ, (2) 7-or-more reporting stations, and (3) the standard error of the

145 energy fit < 30% of the reported stroke energy. However, not every reporting station will provide
146 an energy measurement. In extreme cases, a 7-station event might include only 1 or 2 energy
147 measurements. Our analyses of the WWLLN events indicate that Holzworth et al. (2019) further
148 remove events with only one station providing an energy measurement. We will use the same
149 filtering in this study, but we will consider WWLLN data from April 2009 through 2022.

150 2.2 The FORTE Photodiode Detector (PDD)

151 The PDD was a silicon photodiode detector that recorded broadband (0.4–1.1 μm) optical
152 waveforms produced by transient events across its 80° circular Field of View (FOV) below the
153 FORTE satellite. It had a sampling interval of 15 μs and was usually operated in its self-
154 triggering mode where it reported 1.9 ms of data in each record. The PDD had three known
155 issues that impact its ability to detect superbolts.

156 First, each event was followed by a period of dead time that was comparable to the record
157 length. If the PDD triggers on the initial activity within the cloud before a CG, for example, any
158 portion of the CG pulse that occurs during the dead time would be lost. Second, the PDD was
159 designed to turn off during high rates of successive triggers to conserve memory during episodes
160 of glint off the spacecraft or bodies of water. Once a trigger count threshold was reached (often
161 10) over a short time interval (often 40 ms), the instrument would stop triggering until the next
162 pulse-per-second signal. This prevented the PDD from resolving optical pulses that occurred late
163 (hundreds of milliseconds) into long-lasting lightning flashes.

164 Third, the PDD could trigger on energetic particle impacts on the instrument, particularly
165 over the South Atlantic Anomaly (SAA). Unlike the lightning imager on FORTE, the PDD had
166 the ability to natively screen for these energetic particle impacts using an onboard filter. In its
167 self-triggering mode, the PDD only generated events when the digitized signal exceeded the
168 instrument threshold for a prescribed number of consecutive samples. The sample count
169 threshold was commandable between 0 and 31, and usually set to 5 (corresponding to 75 μs).
170 However, this filter was not uniformly applied throughout the FORTE mission. To mitigate
171 residual contamination, we emulate the 5-sample threshold in post-processing to remove
172 energetic particle spikes.

173 After filtering the PDD data, we identify the WWLLN strokes associated with PDD
174 events. We first subset the daily catalog of WWLLN strokes to identify those that occur near the
175 FORTE satellite subpoint around the time of the PDD event. Once we have the candidate list, we
176 compute the Time Of Flight (TOF) of the corresponding optical signals from each WWLLN
177 stroke to FORTE. Finally, we compare the TOF-corrected event times to the PDD event times.
178 To account for potential physical and scattering delays in the optical signals (Suszcynsky et al.,
179 2000; Peterson, 2022), we consider any event that occurs within the millisecond before the PDD
180 trigger time to be a valid match. We only include PDD events matched with single WWLLN
181 strokes in our analyses.

182 2.3 The Geostationary Lightning Mapper (GLM)

183 GLM is a pixelated lightning imager that records the scene below the GOES satellites in
184 a narrow spectral band (777.4 nm) and triggers on transient increases in pixel energies during 2-

185 ms integration frames. Individual pixel detections are referred to as “events” in the GLM
186 parlance, and they are clustered into larger-scale features that approximate lightning processes
187 (Mach, 2020). Clusters of events in the same integration frame that form a contiguous region on
188 the GLM imaging array are termed “groups” and approximate optical pulses. Groups that occur
189 in close proximity in space and time are then clustered into features approximating lightning
190 flashes using a Weighted Euclidian Distance (WED) model. GLM flashes and their constituent
191 features are also used to generate meteorological imagery (Bruning et al., 2019) that provides
192 additional context for GLM and WWLLN detections.

193 We do not use the operational GLM data products, however. These datasets provided by
194 NOAA are degraded by hard limits coded into the GLM ground system software that split large
195 or long-lasting flashes into pieces. Instead, we have created a repaired version of the GLM
196 cluster feature data that mitigates these issues (Peterson, 2019). We also use this repaired dataset
197 to construct meteorological GLM imagery. Our gridded products further differ from those in
198 Bruning et al. (2019) because they are based on group-level rather than event-level data to reduce
199 biases from radiative transfer effects across the cloud scene (Peterson et al., 2017; Peterson,
200 2021a). We use GOES-16 data from 2018 to 2022 and GOES-17 data from 2019-2022 matched
201 with WWLLN events in this study. However, our analysis of GLM superbolts focuses on
202 observations from both satellites during the year 2020.

203 Due to a combination of GLM parallax (Virts and Koshak, 2020), WWLLN location
204 uncertainties, and phenomenological differences, GLM often reports no lightning at the locations
205 of WWLLN high energy events during the 15-minute data packet associated with the WWLLN
206 stroke. Rather than match WWLLN strokes to GLM groups, we place our focus on linking these
207 WWLLN events to their parent thunderstorm region. We accomplish this by identifying the
208 nearby (i.e., within 0.25 degrees) gridpoint with the greatest value in the Flash Extent Density
209 (FED: Lojou and Cummins, 2004) imagery product. FED is a spatial representation of GLM
210 flash rates, and this peak value should correspond to the most active thunderstorm region in the
211 vicinity of the WWLLN stroke.

212

213 **3 Results**

214 **3.1 WWLLN Energies from FORTE PDD Events including Superbolts**

215 The FORTE PDD is the best available analog for comparing the energies reported by
216 WWLLN with optical outputs compatible with Turman (1977)’s study because it was a
217 broadband sensor with a large dynamic range. GLM is not ideal because it measures narrowband
218 energies integrated over milliseconds, while space-based photometers saturate before reaching
219 the superbolt threshold.

220 The scatterplots in Figure 1 compare FORTE PDD peak optical powers (Figure 1a) and
221 total optical energies (Figure 1b) with WWLLN energies during the last year of the PDD record.
222 All single-matched WWLLN events are shown in light blue, while only cases that pass the filters
223 used by Holzworth et al. (2019) are shown in dark blue. The PDD recorded 24 superbolts
224 matched with WWLLN events during this period, including four 300 GW cases. The WWLLN

225 strokes in 8 superbolt events passed Holzworth et al. (2019)'s quality filters. Yet, the energies
226 reported by WWLLN for these superbolts are quite low, ranging from 700 J to 2×10^4 J – two
227 orders of magnitude or more below the WWLLN high energy event threshold.

228 While there is a positive correlation between WWLLN VLF energies and both peak
229 optical power and total optical energy that can be noted in Figure 1a and b, the upward slopes are
230 insufficient to reach the WWLLN energy threshold within the range of optical events that have
231 been recorded from lightning. Moreover, the top matched WWLLN events produce optical
232 outputs well below expectations for a superbolt event.

233 The FORTE PDD data confirm that energetic WWLLN events are responding to a
234 different set of physical mechanisms than optical superbolts, and we should not expect one to
235 imply the other – even if they have a similar pattern of occurrence.

236 3.2 The Most Energetic WWLLN and GLM Lightning

237 We analyzed the top GLM superbolt cases in our quality-controlled database from the
238 year 2020 and all quality-filtered WWLLN energetic events > 1 MJ from 2018 to 2022. We
239 found that these two different types of energetic lightning occurred in conflicting meteorological
240 contexts. The top GLM superbolt shown in Figure 2 is demonstrative of GLM superbolts. Figure
241 2a shows the structure of the flash (greyscale line segments), the location of the superbolt
242 (yellow circle), and locations of WWLLN strokes in all ongoing flashes at the time of the
243 superbolt (white stars) overlaid on top of GOES-16 Advanced Baseline Imager (ABI: Schmit et
244 al., 2018) $10.3 \mu\text{m}$ infrared brightness temperature imagery. The domain of the plot is chosen to
245 encompass the lightning-producing portion of the storm, which is depicted in the meteorological
246 GLM imagery products shown in Figure 2 b-d. Flash Extent Density (FED) spatial flash rates are
247 shown in Figure 2b. Mean flash extent (measured between the most distant points in each flash)
248 is shown in Figure 2c. Mean flash duration is shown in Figure 2d. The ABI imagery is preserved,
249 but changed to greyscale in these plots.

250 This 7.3 MJ GLM superbolt occurred midway through a long-horizontal GLM megaflash
251 spanning 242 km between its most distant points. This flash produced 6 WWLLN strokes along
252 its path beginning in the northeast and propagating south and west along multiple branches, as
253 depicted in Figure 1a. The superbolt was located in a region of low flash rates (Figure 2b), large
254 flash extents (Figure 2c), and long flash durations (Figure 2d) consistent with electrified
255 stratiform clouds. By contrast, the active convective cells in the storm (to the north and west)
256 produce frequent small / short-lived flashes.

257 The GLM light curve from this flash is shown in Figure 2e with the superbolt (yellow
258 circle) and only the WWLLN strokes associated with the flash (white stars) overlaid. The GLM
259 superbolt coincided with a WWLLN stroke, but the VLF energy from this extreme optical event
260 was only $\sim 10^4$ J – two orders of magnitude below the WWLLN threshold. As we saw with the
261 FORTE PDD, extreme optical emission does not correlate with exceptional VLF energies.

262 Instead, our survey of all quality controlled WWLLN high energy event cases during the
263 public GLM data record reveals a different origin for these exceptional lightning discharges. The
264 top case – a 6.7 MJ WWLLN stroke – is shown in Figure 3 and is representative of these events.

265 Instead of large megaflashes that are well-resolved by GLM, WWLLN high energy events occur
266 in small convective flashes. Due to the small size of the flash in Figure 3, we replaced its
267 horizontal structure (line segments in Figure 2) with black dots depicting the group centroid
268 locations. We also included raw level-0 events (white dots), some of which are removed in level-
269 2 filtering (grey dots).

270 The WWLLN high energy event occurred simultaneously with two additional WWLLN
271 strokes located to the west and south in Figure 3a. As these additional strokes lacked energy
272 measurements, we position them at 100 J in Figure 3e out of convenience. However, we
273 speculate that they may be artifacts of the WWLLN geolocation algorithm caused by the high-
274 energy event having a complex waveform shape. Interrogation of the station waveform data
275 would be required to confirm, but this data is not preserved for longer than a few days
276 (Holzworth et al., 2019).

277 Regardless, the WWLLN high energy event location in Figure 3 is co-located with the
278 coldest cloud-tops in the thunderstorm, representing an intense updraft. Usually, strong
279 convection generates frequent small discharges (Bruning and MacGorman, 2013) that are
280 constantly neutralizing the charge separation generated by the updraft. In this WWLLN high
281 energy event case, the flash sizes and durations are consistent with ordinary convection, but the
282 FED values in Figure 3b are quite low.

283 The WWLLN high energy event occurred at the beginning of the GLM flash. The
284 coherency filter in the GLM level-2 software rejects the first group in all flashes. These removed
285 events are preserved at level-0 (white dots) and are no more energetic than the events later in the
286 flash. This is consistent with other cases where the WWLLN high energy event is separated by
287 up to hundreds of milliseconds from the nearest GLM activity and, when there is coincidence
288 with GLM groups, their optical energies are modest at best. As with the FORTE PDD, none of
289 the WWLLN high energy events that we examined are also GLM superbolts.

290 3.3 Meteorological Context of WWLLN High Energy Events and GLM Superbolts

291 To generalize the findings of our case analysis, we compiled statistics for the GLM
292 gridded products associated with WWLLN high energy events and GLM superbolts using a 1 MJ
293 threshold in either case. Statistics of the gridded products shown in Figures 2 and 3 are presented
294 in Figure 4: Flash Extent Density (Figure 4a), mean flash extent (Figure 4b), and mean flash
295 duration (Figure 4c). These histograms indicate that the cases in Figures 2 and 3 are
296 representative of the broader trends. WWLLN high energy events originate in storm regions that
297 have distinctly smaller and short-lived flashes compared to superbolts – consistent with
298 convection – but also with low flash rates that are comparable to stratiform clouds. Animating
299 the plots of WWLLN high energy events like Figure 3 (omitted for brevity) clarifies that the low
300 flash rates in Figure 4a arise from storms that are either decaying (as in Figure 3) or starting to
301 produce lightning (including after a pause in GLM / WWLLN detections).

302 While future work is required to identify the source of the intense VLF emissions, our
303 initial analyses show that WWLLN high energy events could represent a unique class of
304 convective discharge that would merit its own term. In the meantime, we speculate two possible
305 origins for these events. First, they could be a kind of discharge that radiates strongly in the VLF

306 but not optical, like CIDs to VHF. Second, they could be related to the changing thunderstorm
307 dynamics permitting more charge than usual to be amassed before the WWLLN stroke.

308

309 **4 Conclusions**

310 After comparing the VLF energies reported by WWLLN with measurements from two
311 optical instruments – the PDD on the FORTE satellite, and GLM – we conclude that WWLLN
312 high energy events are not optical superbolts. Optical superbolts are associated with long-
313 horizontal lightning flashes in low flash rate regions outside of the convective core of the
314 thunderstorm. The WWLLN energies from superbolts are not remarkable – $10^3 - 10^5$ J, but
315 notably less than the 10^6 J WWLLN high energy event threshold. By contrast, WWLLN high
316 energy events occur within convective storm regions with low flash rates despite the otherwise
317 typical prevalence of small, short-lived flashes and overshooting top signatures marking intense
318 updrafts in the ABI infrared imagery.

319 Based on these observations, we hypothesize that the extreme VLF energies reported by
320 WWLLN may arise in two ways. The first is a possible yet-to-be identified discharge that
321 radiates strongly in the VLF but not optical. The second is the changing thunderstorm dynamics
322 permitting an unusual amount of charge to be stored between convective flashes, which is then
323 neutralized during the high energy WWLLN stroke. This could explain the prominence of high
324 peak current negative polarity strokes in Holzworth et al. (2019), while the limited sizes of
325 convective flashes explain the lack of intense optical output. We need additional measurements
326 of thunderstorms producing WWLLN high energy events to determine whether this hypothesis is
327 valid. In any case, WWLLN high energy events appear to correspond to a unique class of
328 discharge distinct from optical superbolts.

329

330 **Acknowledgments**

331 Los Alamos National Laboratory is operated by Triad National Security, LLC, under contract
332 number 89233218CNA000001.

333

334 **Open Research**

335 The FORTE PDD and GLM superbolt data used in this study are available at the Harvard
336 Dataverse via DOI: 10.7910/DVN/RV39JT, (Peterson, 2020). Reprocessed GLM data are
337 available from the NASA Global Hydrometeorology Resource Center DAAC at DOI:

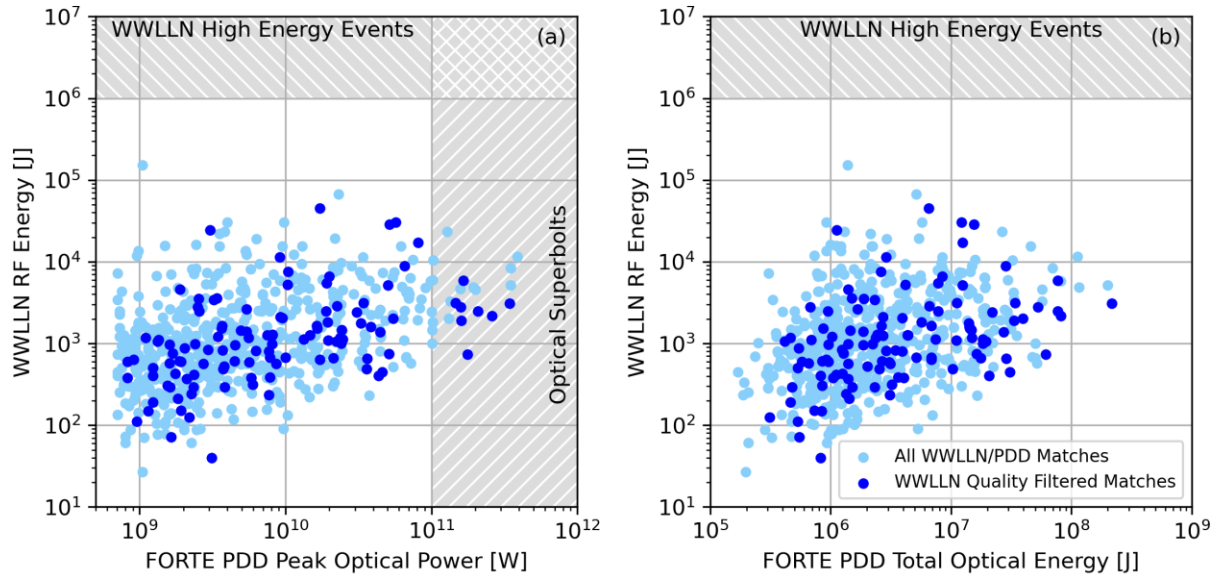
338 10.5067/GLM/CIERRA/DATA101 (Peterson, 2021b). The University of Washington maintains
 339 a list of WWLLN high energy strokes at <http://wwlln.net/publications/LargeStrokes.txt>.

340

341 References

- 342 Abarca, S. F., Corbosiero, K. L., & Galarneau Jr, T. J. (2010). An evaluation of the worldwide
 343 lightning location network (WWLLN) using the national lightning detection network
 344 (NLDN) as ground truth. *Journal of Geophysical Research: Atmospheres*, *115*(D18).
 345 Albrecht, R. I., Goodman, S. J., Buechler, D. E., Blakeslee, R. J., & Christian, H. J. (2016).
 346 Where are the lightning hotspots on Earth?. *Bulletin of the American Meteorological*
 347 *Society*, *97*(11), 2051-2068.
- 348 Bruning, E. C., & MacGorman, D. R. (2013). Theory and observations of controls on lightning
 349 flash size spectra. *Journal of the Atmospheric Sciences*, *70*(12), 4012-4029.
- 350 Bruning, E. C., Tillier, C. E., Edgington, S. F., Rudlosky, S. D., Zajic, J., Gravelle, C., ... &
 351 Meyer, T. C. (2019). Meteorological imagery for the geostationary lightning mapper.
 352 *Journal of Geophysical Research: Atmospheres*, *124*(24), 14285-14309.
- 353 Christian, H. J., Blakeslee, R. J., Boccippio, D. J., Boeck, W. L., Buechler, D. E., Driscoll, K. T.,
 354 ... & Stewart, M. F. (2003). Global frequency and distribution of lightning as observed
 355 from space by the Optical Transient Detector. *Journal of Geophysical Research:*
 356 *Atmospheres*, *108*(D1), ACL-4.
- 357 Cummins, K. L., & Murphy, M. J. (2009). An overview of lightning locating systems: History,
 358 techniques, and data uses, with an in-depth look at the US NLDN. *IEEE transactions on*
 359 *electromagnetic compatibility*, *51*(3), 499-518.
- 360 Dowden, R. L., Brundell, J. B., & Rodger, C. J. (2002). VLF lightning location by time of group
 361 arrival (TOGA) at multiple sites. *Journal of Atmospheric and Solar-Terrestrial Physics*,
 362 *64*(7), 817-830.
- 363 Holzworth, R. H., McCarthy, M. P., Brundell, J. B., Jacobson, A. R., & Rodger, C. J. (2019).
 364 Global distribution of superbolts. *Journal of Geophysical Research: Atmospheres*,
 365 *124*(17-18), 9996-10005.
- 366 Kirkland, M. W., Suszcynsky, D. M., Guillen, J. L. L., & Green, J. L. (2001). Optical
 367 observations of terrestrial lightning by the FORTE satellite photodiode detector. *Journal*
 368 *of Geophysical Research: Atmospheres*, *106*(D24), 33499-33509.
- 369 Light, T. E. L. (2020). A retrospective of findings from the FORTE satellite mission. *Journal of*
 370 *Geophysical Research: Atmospheres*, *125*(9), e2019JD032264.
- 371 Light, T. E. L., & Jacobson, A. R. (2002). Characteristics of impulsive VHF lightning signals
 372 observed by the FORTE satellite. *Journal of Geophysical Research: Atmospheres*,
 373 *107*(D24), ACL-8.
- 374 Lojou, J.-Y., & Cummins, K. L. (2004). On the representation of two- and three-dimensional
 375 total lightning information. In Preprints, Conference on Meteorological Applications of
 376 Lightning Data, Paper 2.4, AMS Annual Meeting, San Diego, CA, USA.
- 377 Mach, D. M. (2020). Geostationary Lightning Mapper clustering algorithm stability. *Journal of*
 378 *Geophysical Research: Atmospheres*, *125*(5), e2019JD031900.

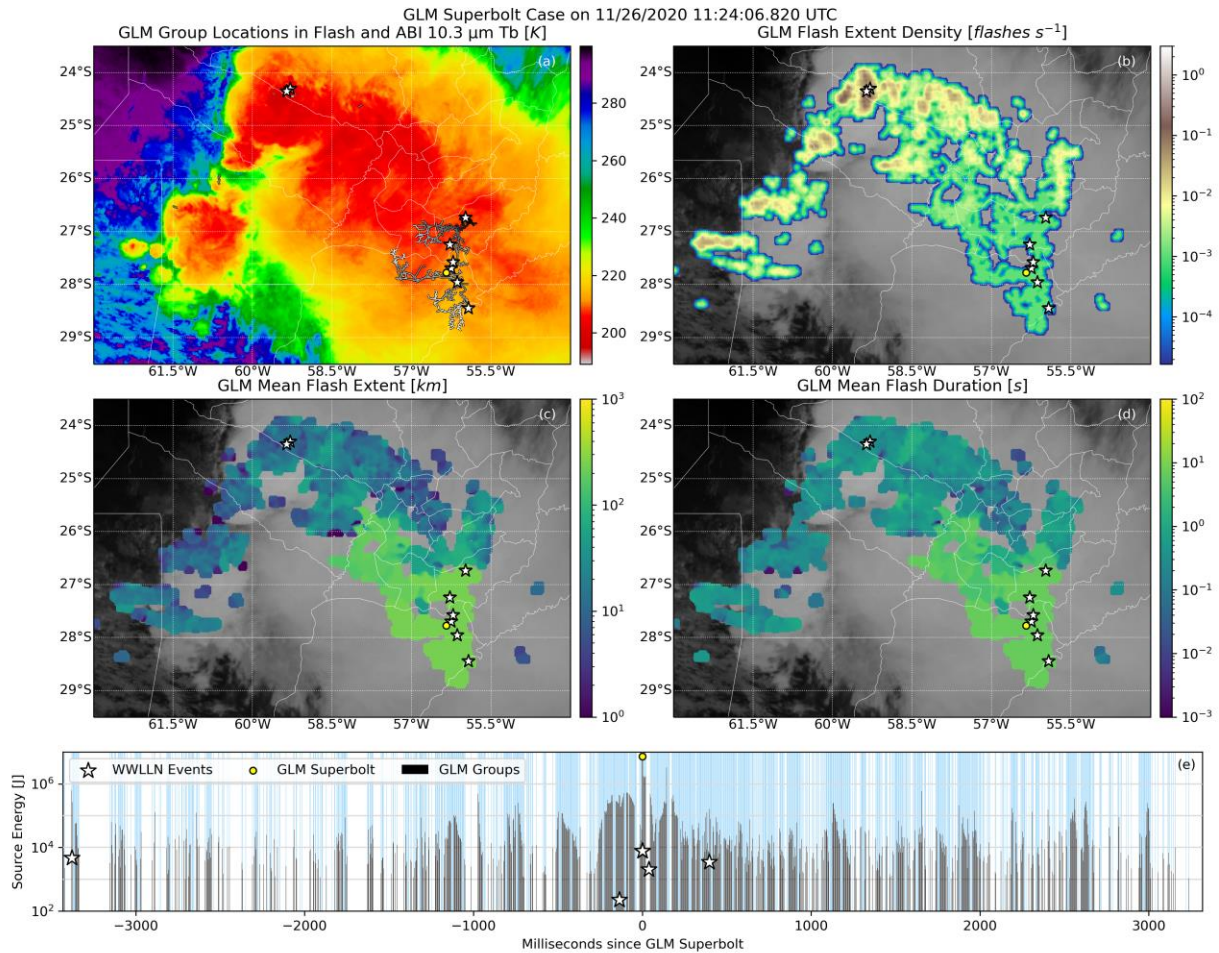
- 379 Peterson, M. (2019). Research applications for the Geostationary Lightning Mapper operational
380 lightning flash data product. *Journal of Geophysical Research: Atmospheres*, 124(17-18),
381 10205-10231.
- 382 Peterson, M. (2020). Lightning Superbolt Data, <https://doi.org/10.7910/DVN/RV39JT>, Harvard
383 Dataverse, V2.
- 384 Peterson, M. (2021a). Holes in optical lightning flashes: Identifying poorly transmissive clouds
385 in lightning imager data. *Earth and Space Science*, 8(2), e2020EA001294.
- 386 Peterson, M. (2021b). GLM-CIERRA. <https://doi.org/10.5067/GLM/CIERRA/DATA101>
- 387 Peterson, M. (2022). FORTE measurements of global optical lightning waveforms and
388 implications for optical lightning detection. *Earth and Space Science*, 9(6),
389 e2022EA002280.
- 390 Peterson, M., & Liu, C. (2011). Global statistics of lightning in anvil and stratiform regions over
391 the tropics and subtropics observed by the Tropical Rainfall Measuring Mission. *Journal*
392 *of Geophysical Research: Atmospheres*, 116(D23).
- 393 Peterson, M., Rudlosky, S., & Deierling, W. (2017). The evolution and structure of extreme
394 optical lightning flashes. *Journal of Geophysical Research: Atmospheres*, 122(24), 13-
395 370.
- 396 Peterson, M., & Kirkland, M. W. (2020). Revisiting the detection of optical lightning superbolts.
397 *Journal of Geophysical Research: Atmospheres*, 125(23), e2020JD033377.
- 398 Peterson, M., & Lay, E. (2020). GLM observations of the brightest lightning in the Americas.
399 *Journal of Geophysical Research: Atmospheres*, 125(23), e2020JD033378.
- 400 Peterson, M., Mach, D., & Buechler, D. (2021). A global LIS/OTD climatology of lightning
401 flash extent density. *Journal of Geophysical Research: Atmospheres*, 126(8),
402 e2020JD033885.
- 403 Rudlosky, S. D., Goodman, S. J., Virts, K. S., & Bruning, E. C. (2019). Initial geostationary
404 lightning mapper observations. *Geophysical Research Letters*, 46(2), 1097-1104.
- 405 Schmit, T. J., Lindstrom, S. S., Gerth, J. J., & Gunshor, M. M. (2018). Applications of the 16
406 spectral bands on the Advanced Baseline Imager (ABI).
- 407 Suszcynsky, D. M., Kirkland, M. W., Jacobson, A. R., Franz, R. C., Knox, S. O., Guillen, J. L.
408 L., & Green, J. L. (2000). FORTE observations of simultaneous VHF and optical
409 emissions from lightning: Basic phenomenology. *Journal of Geophysical Research:*
410 *Atmospheres*, 105(D2), 2191-2201.
- 411 Thomas, R. J., Krehbiel, P. R., Rison, W., Hamlin, T., Boccippio, D. J., Goodman, S. J., &
412 Christian, H. J. (2000). Comparison of ground-based 3-dimensional lightning mapping
413 observations with satellite-based LIS observations in Oklahoma. *Geophysical research*
414 *letters*, 27(12), 1703-1706.
- 415 Thomson, N. R. (2010). Daytime tropical D region parameters from short path VLF phase and
416 amplitude. *Journal of Geophysical Research: Space Physics*, 115(A9).
- 417 Turman, B. N. (1977). Detection of lightning superbolts. *Journal of Geophysical Research*,
418 82(18), 2566-2568.
- 419 Virts, K. S., & Koshak, W. J. (2020). Mitigation of geostationary lightning mapper geolocation
420 errors. *Journal of Atmospheric and Oceanic Technology*, 37(9), 1725-1736.
- 421 Whipple, F. J. W. and Scrase, F. J. (1936). Point-discharge in the electric field of the Earth.
422 *Geophys. Mem. VII*, 68, 1-20.
- 423 Williams, E. R. (2005). Lightning and climate: A review. *Atmospheric research*, 76(1-4), 272-
424 287.



425
 426 **Figure 1.** Two-dimensional histograms of the (a) peak optical power and (b) total optical energy
 427 of PDD events matched to single WWLLN strokes and WWLLN VLF source energies. PDD
 428 measurements have been normalized to the source, as in Turman (1977). All WWLLN strokes
 429 are shown in light blue, while strokes meeting the filters used in Holzworth et al. (2019) are
 430 shown in dark blue.

431

432



433

434 **Figure 2.** GOES-16 observations of the top GLM superbolt case during the year 2020. GLM (a)

435 group-derived flash structure (greyscale lines representing time, with darker signifying older),

436 (b) Flash Extent Density, (c) mean flash extent, and (d) mean flash duration are overlaid on top

437 of ABI 10.3 μm infrared imagery (color contours in a, greyscale in b-d). WWLLN strokes

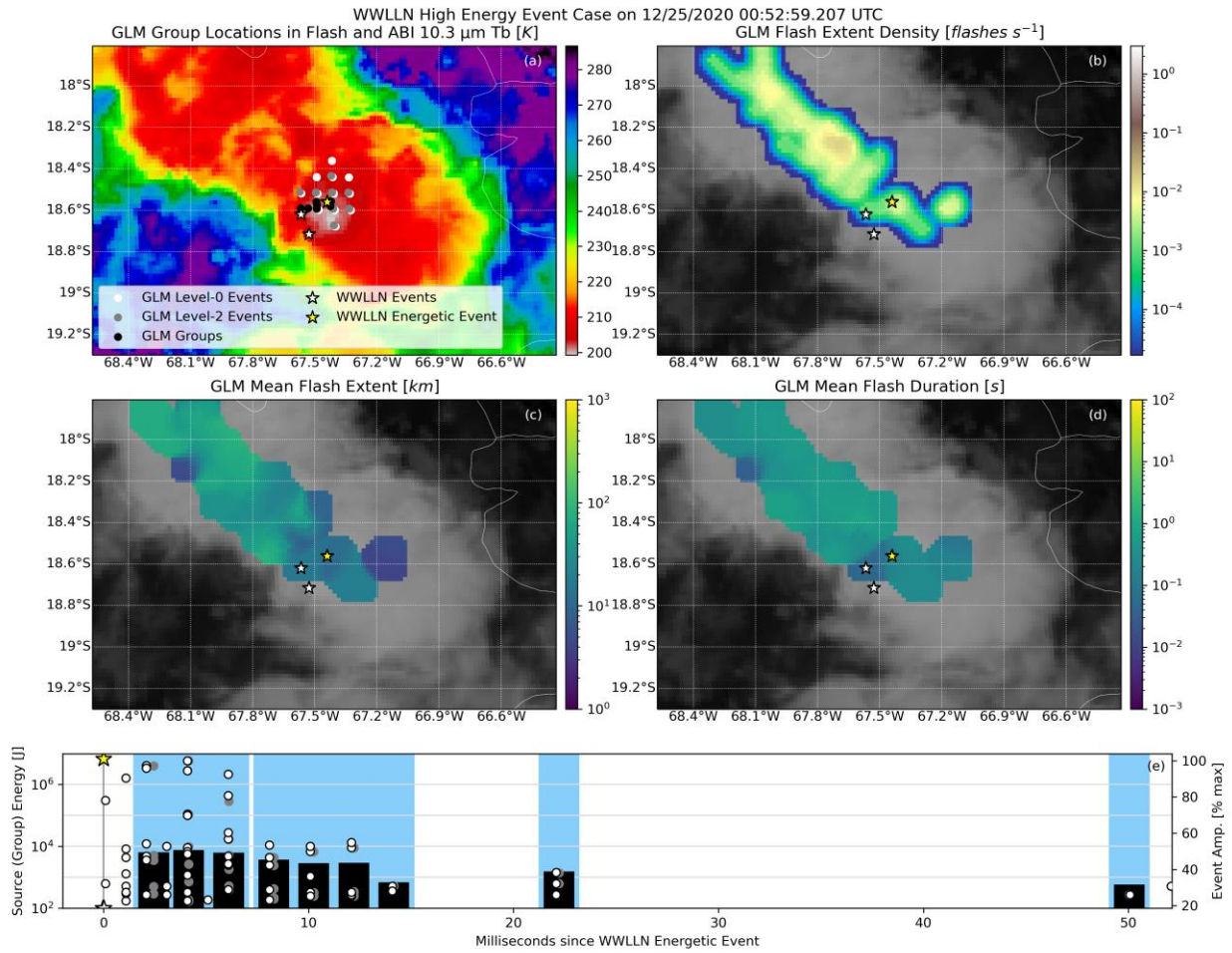
438 around the time of the superbolt are overlaid with star symbols. The superbolt location is

439 indicated with a yellow circle. (e) GLM light curve for the superbolt-producing flash. Groups

440 (grey) are plotted according to their optical energies on top of a blue background highlighting the

441 frame. WWLLN strokes (stars) in the flash are plotted according to their VLF energies.

442



443

444

Figure 3. As in Figure 1, but showing the top WVLLN high energy event during the GLM

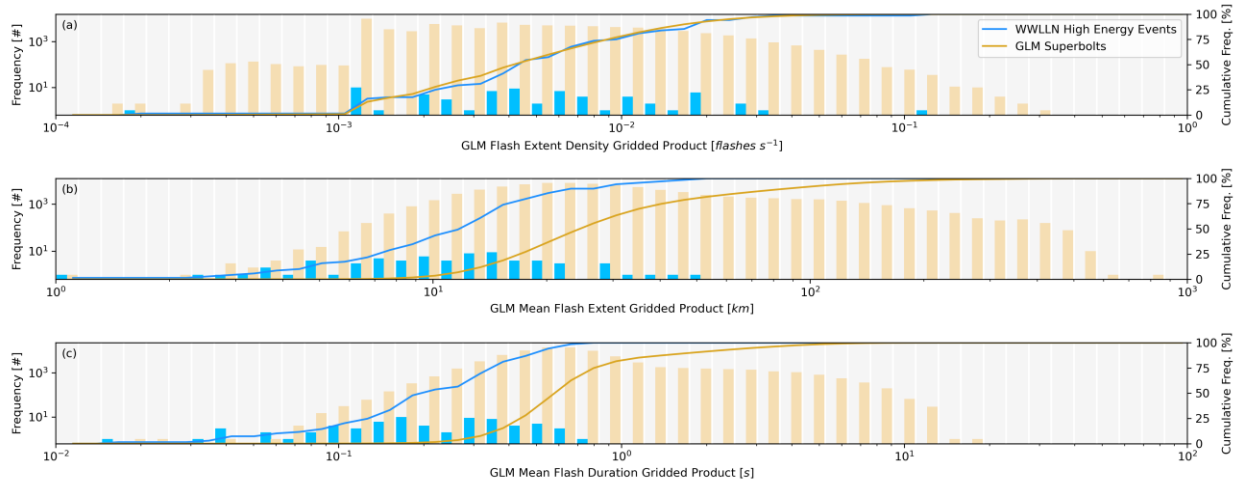
445

public data record. The WVLLN high energy event is colored yellow. GLM raw level-0 (white

446

circles) and filtered level-2 (grey circles) events are also overlaid in (a) and (e).

447



448

449 **Figure 4.** Histograms of the GLM (a) Flash Extent Density, (b) mean flash extent, and
 450 flash duration gridded products corresponding to GLM superbolts (blue) and WWLLN high
 451 energy events (wheat).

452